01 Feb 2009

Small-Signal Impedance Measurement of Power-Electronics-Based AC Power Systems Using Line-to-Line Current Injection

Jing Huang

Keith Corzine
Missouri University of Science and Technology

M. Belkhayat

Recommended Citation

J. Huang et al., "Small-Signal Impedance Measurement of Power-Electronics-Based AC Power Systems Using Line-to-Line Current Injection," *IEEE Transactions on Power Electronics*, Institute of Electrical and Electronics Engineers (IEEE), Feb 2009.
The definitive version is available at https://doi.org/10.1109/TPEL.2008.2007212

Small-Signal Impedance Measurement of Power-Electronics-Based AC Power Systems Using Line-to-Line Current Injection

Jing Huang, *Student Member, IEEE*, Keith A. Corzine, *Member, IEEE*, and Mohamed Belkhayat

***Abstract*—Naval ships as well as aerospace power systems are incorporating a greater degree of power electronic switching sources and loads. Although these components provide exceptional performance, they are prone to instability due to their high efficiency and constant power characteristics that can exhibit negative impedance nature at certain frequencies. When designing these systems, integrators must consider the impedance versus frequency at an interface (which designates source and load). Stability criteria have been developed in terms of source and load impedances for both dc and ac systems, and it is often helpful to have techniques for impedance measurement. For dc systems, the measurement techniques have been well established. This paper introduces a new method of impedance measurement for three-phase ac systems. By injecting an unbalanced line-to-line current between two lines of the ac system, all impedance information in the traditional synchronous reference frame $d-q$ model can be determined. For medium-voltage systems, the proposed technique is simpler and less costly than having an injection circuit for each phase. Since the current injection is between only two phase lines, the proposed measurement device can be used for both ac and dc interfaces. Simulation and laboratory measurements demonstrate the effectiveness of this new technique.**

***Index Terms*—Impedance measurement, power conversion, power system stability, power system testing.**

I. Introduction

POWER-ELECTRONIC-BASED systems are prone to negative impedance instability due to the constant-power nature of the individual components [1]–[13]. Previous research has shown that the instabilities can be avoided in some systems by modification of the power electronic controls [4]. Other research has defined admittance space criteria based on a dc interface that can be used to design system components [5]. In 1976, Middlebrook first stated the criterion that a system is stable if the Nyquist contour of product of the source impedance Z_s and load admittance Y_l remains within the unit circle [1]. Since then, impedance techniques have been used for power supply design [2], [3], and a number of stability criteria have been proposed [5], [7], [8] that involve magnitude and phase of the impedance. When power components from various vendors are integrated into a system, their impedances can be used to determine the overall system stability. For this reason, extraction of impedance is becoming increasingly important in many applications.

Methods of extracting impedance in dc systems have been well established [4]–[10], whereby small disturbance signals at various frequencies are injected into the system, and the pertinent currents and voltages are measured and processed to obtain the desired impedance or admittance over the frequency range of interest. The disturbance injection may be a shunt current or a series voltage. For ac systems, the traditional current-injection techniques need to be applied in the synchronous $d-q$ reference frame. Recent research has shown that stability criteria for ac systems can be developed based on the $d-q$ impedances of the source and load (defined at a particular system interface) [12]. Initial research into ac impedance measurement was based on injecting current disturbances using suppressed-carrier modulation [13]. Other research has focused on impedance measurement techniques on ac power systems [14], [15]. In the $d-q$ reference frame, suppressed-carrier modulation is equivalent to injecting a disturbance current at the frequency of interest with constant amplitude. By adjusting the modulation of linear amplifiers, one could inject disturbances into the d- and then q-axes to obtain the impedance information [13]. In later research, specific current-injection circuits were proposed with medium-voltage systems in mind [16]. In particular, chopper circuits, pulsewidth modulation (PWM) amplifiers, and additional electric machines were proposed for performing the current injection. Furthermore, injecting signals at arbitrary angles (not completely in the d- or q-axis) was suggested to account for the effect of coupling between the axes [16].

This paper proposes an alternative method for measuring the $d-q$ model impedances of an ac power system. Instead of using a three-phase current-injection circuit, a single-phase current is injected between two of the ac lines. Compared with existing measurement techniques, the proposed method has the following advantages.

1) It is simpler to construct and requires less power electronic components that will reduce the cost, especially in medium-voltage systems.
2) The transistors are switched asynchronously using square waves with a fixed 50% duty cycle, which makes the implementation straightforward.
3) The structure can be used to measure impedance on both ac and dc systems.

Manuscript received December 31, 2007; revised August 7, 2008. Current version published February 6, 2009. This paper was presented at the 2006 IEEE Industry Applications Society Conference. Recommended for publication by Associate Editor Andrzej M. Trzynadlowski.

J. Huang and K. A. Corzine are with Missouri University of Science and Technology, Rolla, MO 65409 USA (e-mail: keith@corzine.net).

M. Belkhayat is with Northrop Grumman Newport News, Washington, DC, WA 20003 USA.

Digital Object Identifier 10.1109/TPEL.2008.2007212

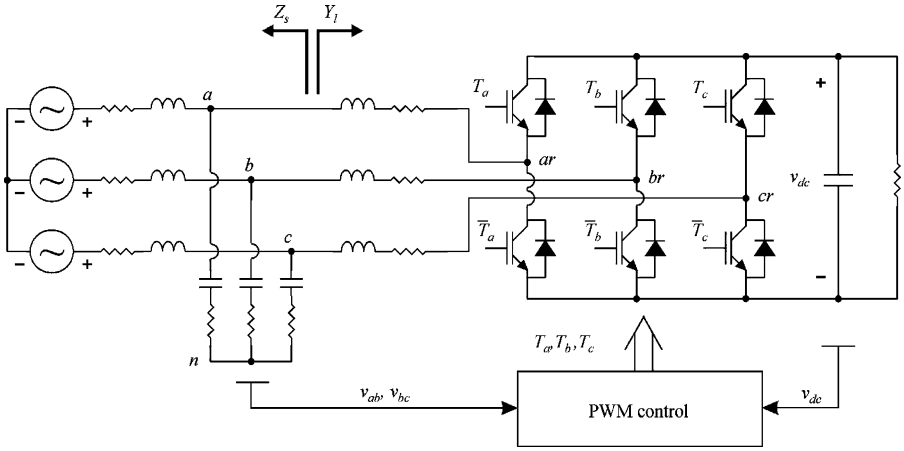

Fig. 1. Example active rectifier system.

4) Each measurement point is made from two different frequencies that avoids the necessity to align the measurements with the d- or q-axis.

The theoretical background for the proposed line-to-line injection ac impedance measurement is presented. This is followed by the introduction of practical current injection circuits. The new technique is then demonstrated with detailed computer simulation and laboratory measurements.

II. Stability Analysis and Impedance

Middlebrook [1] stated the criterion that a system is stable if the Nyquist contour of the product of source impedance and load admittance $Z_s Y_l$ remains within the unit circle. Since then, considerable research on impedance/admittance extraction has been conducted for dc systems. Extraction of impedance/admittance in dc systems is relatively simple due to natural existence of the system's equilibrium point. A small voltage or current disturbance at a specific frequency is injected to obtain the small-signal impedance ($Z = \Delta v/\Delta i$). Stability performance over the frequency range of interest could be obtained by repeating this procedure and analyzing the Nyquist plot of $Z_s Y_l$.

For symmetrical and balanced three-phase ac systems, an equilibrium point can be obtained from the *d–q* model. When all quantities are transformed into the synchronous $d-q$ reference frame, the small-signal $d-q$ impedance characteristics of a source or load describe the frequency-dependent relationship between small variations of $d-q$ voltages and $d-q$ currents in the same way as with dc systems. In the case of ac systems, the impedance is expressed in a matrix by

$$\begin{bmatrix} \Delta V_q \\ \Delta V_d \end{bmatrix} = \begin{bmatrix} Z_{qq} & Z_{qd} \\ Z_{dq} & Z_{dd} \end{bmatrix} \begin{bmatrix} \Delta I_q \\ \Delta I_d \end{bmatrix} \tag{1}$$

where Δ denotes a small deviation of the respective variable from the equilibrium point.

Fig. 1 shows an example active rectifier system used to illustrate concepts of stability and impedance in three-phase ac systems. For simplicity, a 60-Hz ac power source with a resistor and inductor is used to represent a utility grid or a synchronous generator. A PWM filter is located before the full-bridge insulated gate bipolar transistor (IGBT) rectifier. Constant-power load performance is achieved by keeping the dc bus voltage $v_{\rm dc}$ constant across the resistive load. The rectifier control also maintains unity power factor at the source terminals. A shunt current will be injected between the PWM filter and the rectifier, which is the interface-defined source and load in this ac system.

Fig. 2 shows an analysis of the active rectifier system. An average-value model of the PWM was used for this analysis. Using this model, the source and load impedance matrices can be obtained. For light loads, the Nyquist plot indicates stability, as shown in Fig. 2(a). When the load is increased, an encirclement of the -1 point occurs, as shown in Fig. 2(b). Fig. 2(c) shows a dynamic simulation where the load is stepped from light load to heavy load. As predicted by the Nyquist plot, an instability occurs.

III. Techniques of AC Impedance Extraction

For this research, the injection of shunt current disturbances over series voltage disturbances was selected since this could lead to more practical implementation for medium-voltage systems, considering the ratings of present-day semiconductor devices. In previous research [12], [13], the quadrature amplitude modulation (QAM) of the fundamental, also known as the suppressed-carrier injection technique, was used for impedance measurement. With this method, a set of three-phase modulated currents are injected into the system between the source and load with the form

$$i_{a\rm inj} = I_m \cos(\omega_s t)\cos(\omega_e t - \phi_{\rm inj}) \tag{2}$$

$$i_{b\rm inj} = I_m \cos(\omega_s t)\cos\left(\omega_e t - \frac{2\pi}{3} - \phi_{\rm inj}\right) \tag{3}$$

$$i_{c\rm inj} = I_m \cos(\omega_s t)\cos\left(\omega_e t + \frac{2\pi}{3} - \phi_{\rm inj}\right) \tag{4}$$

where ω_e is the fundamental radian frequency of the system. The injection signals are sinusoidal in the $d-q$ synchronous reference frame with frequency ω_s, which is similar to the small-signal injection signals used in dc systems. In the synchronous

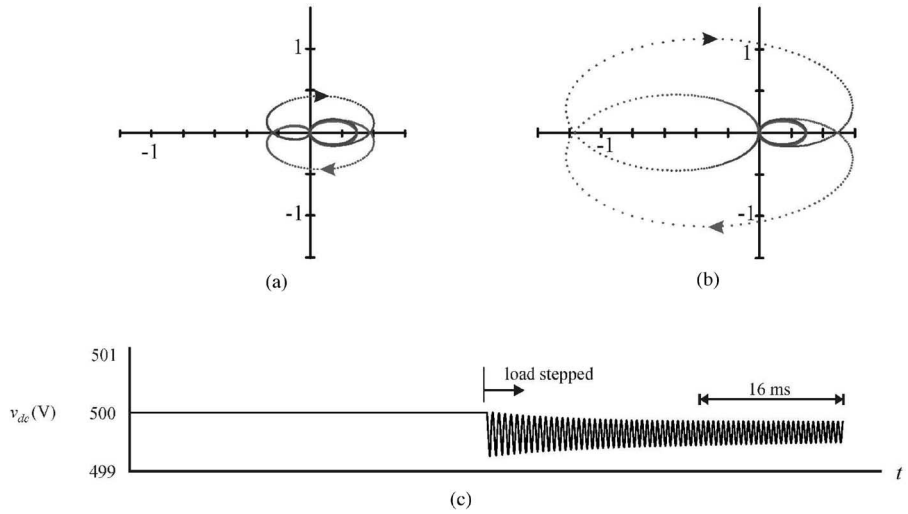

Fig. 2. Nyquist plots and average-value model simulation. (a) Nyquist plot (light load). (b) Nyquist plot (large load). (c) Average-value model simulation.

reference frame, the injected $d-q$ currents are

$$i_{q\mathrm{inj}} = I_m \cos(\omega_s t)\cos(\phi_{\mathrm{inj}}) \tag{5}$$

$$i_{d\mathrm{inj}} = I_m \cos(\omega_s t)\sin(\phi_{\mathrm{inj}}). \tag{6}$$

When the currents are injected in steady state, the source or load impedances are related to the disturbance of voltages and currents in the arbitrary reference frame at the injected frequency by (1).

For a three-phase system without a zero-sequence current, the impedance matrix consists of four unknowns: Z_{qq}, Z_{qd}, Z_{dq}, and Z_{dd}. Therefore, at least two sets of measurements are needed in order to solve the linear system of equations. For the two measurements, the full set of equations is

$$\widetilde{V}_{q1} = Z_{qq}\widetilde{I}_{q1} + Z_{qd}\widetilde{I}_{d1} \tag{7}$$

$$\widetilde{V}_{d1} = Z_{dq}\widetilde{I}_{q1} + Z_{dd}\widetilde{I}_{d1} \tag{8}$$

$$\widetilde{V}_{q2} = Z_{qq}\widetilde{I}_{q2} + Z_{qd}\widetilde{I}_{d2} \tag{9}$$

$$\widetilde{V}_{d2} = Z_{dq}\widetilde{I}_{q2} + Z_{dd}\widetilde{I}_{d2} \tag{10}$$

where $\widetilde{I}$ and $\widetilde{V}$ are the measured phasor currents and voltages at the injection frequency ω_s, respectively, and the subscripts 1 and 2 denote the two linear independent measurements. The equations have a unique solution for the impedance matrix only when the two measurements are linearly independent.

In previous research [16], two different injection angles ϕ_{inj} are used for each injection frequency of interest, resulting in injected currents of

$$i_{q1\mathrm{inj}} = I_m \cos(\omega_s t)\cos(\phi_{1\mathrm{inj}}) \tag{11}$$

$$i_{d1\mathrm{inj}} = -I_m \cos(\omega_s t)\sin(\phi_{1\mathrm{inj}}) \tag{12}$$

$$i_{q2\mathrm{inj}} = I_m \cos(\omega_s t)\cos(\phi_{2\mathrm{inj}}) \tag{13}$$

$$i_{d2\mathrm{inj}} = -I_m \cos(\omega_s t)\sin(\phi_{2\mathrm{inj}}) \tag{14}$$

where $\phi_{1\mathrm{inj}}$ and $\phi_{2\mathrm{inj}}$ are different injection angles. For the same injection frequency, the current amplitude I_m is kept the same for the two different angles. To illustrate this process, the two sets of injected currents in the $d-q$ plane are shown in Fig. 3. It can be seen that the two current vectors are linearly independent, and thus, are suitable to be used to solve the impedance matrix.

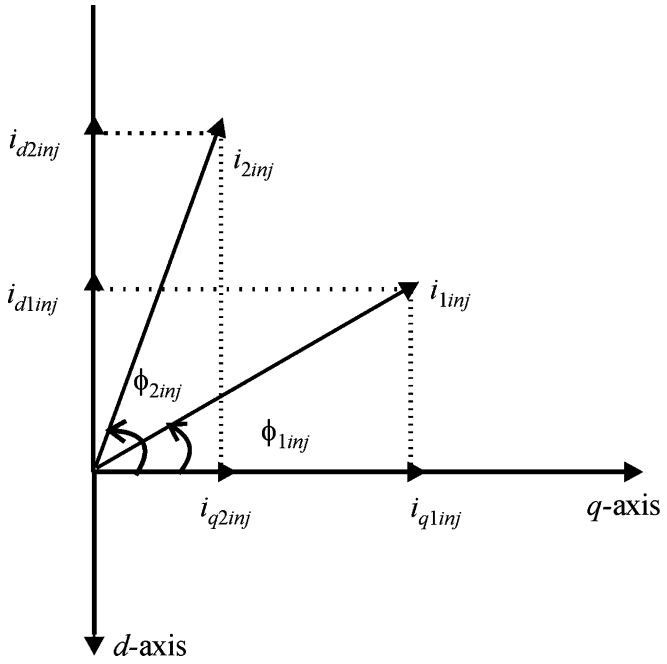

Fig. 3. Vector diagram of three-phase injected currents.

It is instructive to look at other methods of obtaining two independent measurements. The injected signals can be pure sinusoidal in *a–b–c* variables instead of modulated signals as in (2)–(4). In order to obtain pure sinusoidal injected signals in the $d-q$ reference frame, two measurements need to be taken at different injection frequencies: one at $|\omega_s + \omega_e|$ and the other one at $|\omega_s - \omega_e|$ with the phase sequence reversed. One such

example of a set of injected currents is [17]

$$\begin{aligned}
i_{a1\text{inj}} &= I_m \cos(\omega_s t + \omega_e t) \\
i_{b1\text{inj}} &= I_m \cos\left(\omega_s t + \omega_e t - \frac{2\pi}{3}\right) \\
i_{c1\text{inj}} &= I_m \cos\left(\omega_s t + \omega_e t + \frac{2\pi}{3}\right) \\
i_{a2\text{inj}} &= I_m \cos(\omega_s t - \omega_e t) \\
i_{b2\text{inj}} &= I_m \cos\left(\omega_s t - \omega_e t + \frac{2\pi}{3}\right) \\
i_{c2\text{inj}} &= I_m \cos\left(\omega_s t - \omega_e t - \frac{2\pi}{3}\right). \qquad (15)
\end{aligned}$$

Yet another example involves allowing the injection signal to be unbalanced as

$$\begin{aligned}
i_{a1\text{inj}} &= I_m \cos(\omega_s t + \omega_e t) \\
i_{b1\text{inj}} &= I_m \cos(\omega_s t + \omega_e t) \\
i_{c1\text{inj}} &= -2I_m \cos(\omega_s t + \omega_e t) \\
i_{a2\text{inj}} &= \frac{1}{2} I_m \cos(\omega_s t + \omega_e t) \\
i_{b2\text{inj}} &= I_m \cos\left(\omega_s t + \omega_e t - \frac{2\pi}{3}\right) \\
i_{c2\text{inj}} &= -\frac{\sqrt{3}}{2} I_m \sin(\omega_s t + \omega_e t). \qquad (16)
\end{aligned}$$

Alternatively, other unbalanced injection currents, without zero-sequence current, can be injected to extract the impedance. As the earlier examples illustrate, any two sets of injected signals that are linearly independent can be used to obtain the $d-q$ impedance matrix. Besides the injection method described in [13] and [16], there are a number of different forms that the injected currents can take.

The injection currents shown in (17) represent another example of unbalanced injected currents that might be the easiest when it comes to hardware implementation, because one phase current is set to zero

$$\begin{aligned}
i_{a1\text{inj}} &= 0 \\
i_{b1\text{inj}} &= -I_m \cos(\omega_s t + \omega_e t) \\
i_{c1\text{inj}} &= I_m \cos(\omega_s t + \omega_e t) \\
i_{a2\text{inj}} &= 0 \\
i_{b2\text{inj}} &= -I_m \cos(\omega_s t - \omega_e t) \\
i_{c2\text{inj}} &= I_m \cos(\omega_s t - \omega_e t). \qquad (17)
\end{aligned}$$

In this injection scheme, a positive and a negative fundamental frequencies are separately added to the frequency of interest. In the synchronous reference frame, the injected currents include terms at the frequencies $|\omega_s + 2\omega_e|$ and $|\omega_s - 2\omega_e|$. Regarding only the terms at the injection frequency as important, the injected current in the $d-q$ frame can be expressed as

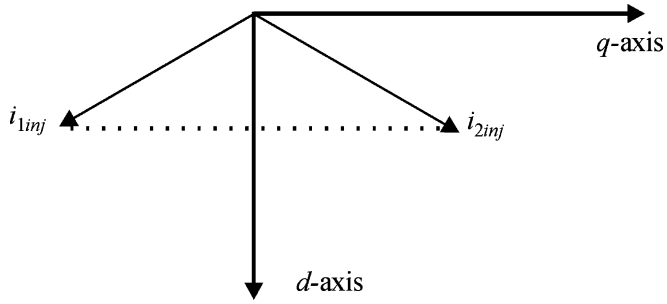

Fig. 4. Vector diagram of line-to-line injected currents.

$$\begin{aligned}
i_{q1\text{inj}} &= \frac{1}{\sqrt{3}} I_m \sin(\omega_s t) + \cdots \\
i_{d1\text{inj}} &= \frac{1}{\sqrt{3}} I_m \cos(\omega_s t) + \cdots \\
i_{q2\text{inj}} &= -\frac{1}{\sqrt{3}} I_m \sin(\omega_s t) + \cdots \\
i_{d2\text{inj}} &= \frac{1}{\sqrt{3}} I_m \cos(\omega_s t) + \cdots. \qquad (18)
\end{aligned}$$

In this method, magnitudes of d- and q-axis terms of the injected currents are maintained while the injected signals are symmetrical about the d-axis. This is illustrated graphically in Fig. 4. It can also be seen that the two current vectors are not directly proportional, which means that they are linearly independent, and thus, can be used to obtain the desired impedance.

Fig. 5 shows a detailed flowchart for measuring a set of impedances in a three-phase ac system. It involves injecting currents of (17) at $|\omega_s + \omega_e|$ and $|\omega_s - \omega_e|$, and capturing steady-state data for each measurement frequency. For ac systems, a line-synchronization program is used to extract the electrical angle information of the fundamental component that will be used to transform all measured currents and voltages to the synchronous $d-q$ reference frame. The disturbance signal is actually the terms at a specific frequency in the frequency domain, so the transformed variables are processed with a fast Fourier transformer (FFT) operation; the magnitude and phase values for each voltage and current value at the injected frequency will be extracted. It should be pointed out that when the frequency is known *a priori*, computational techniques other than FFT, such as Fourier series extraction or discrete Fourier transform (DFT), can also be used [18]. According to the authors' experimentation, the Fourier series extraction yielded nearly the same results as the FFT. The FFT was chosen as a method for this study since the algorithm is readily available in allot of math processing application software packages. The impedances are then calculated from (7)–(10), and the process is repeated for all injection frequencies of interest. By contrast, a dc impedance calculation algorithm is relatively simple. Only one set of captured data is necessary, the $d-q$ transform is not needed, and the impedance is a simple ratio of the voltage and current at the frequency of interest.

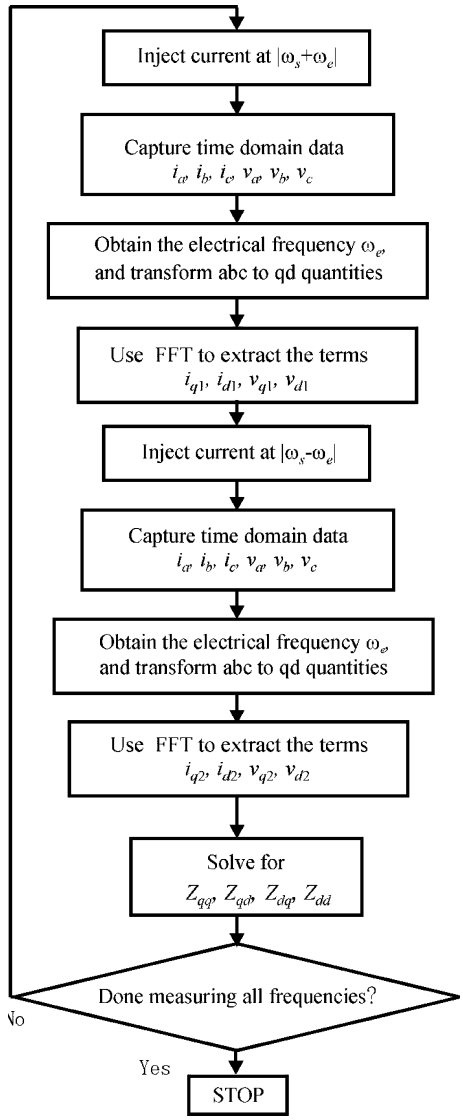

Fig. 5. AC impedance calculation algorithm.

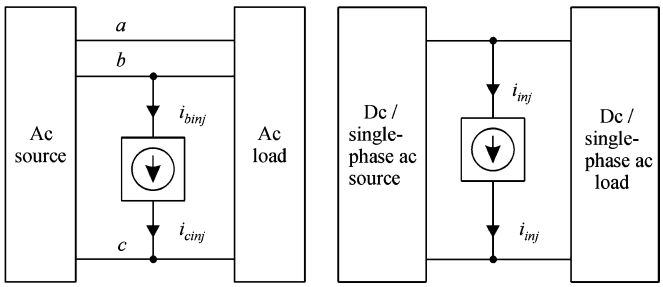

Fig. 6. Practical current injection.

IV. Practical Measurement Circuits

The previous section described several current forms that can be injected to determine the source and load impedances (and thereby the admittance) of three-phase ac systems. As a practical matter, (17) yields a simple way to implement current injection. Since injection currents in only phases b and c are needed and they have opposite signs, a line-to-line injection signal in a three-phase ac system can be used as shown in Fig. 6. Fig. 6 also shows that the injected signal works with dc as well as single-phase ac systems that have a similar structure. Therefore, the injection circuit can be used to measure impedance on both ac and dc systems. The practical measurement can be realized in several ways. Two such circuits are shown in Figs. 7 and 8. It should be noted that the main component of these two circuits is an IGBT that can have characteristics that provide the possibility of application in medium-voltage systems.

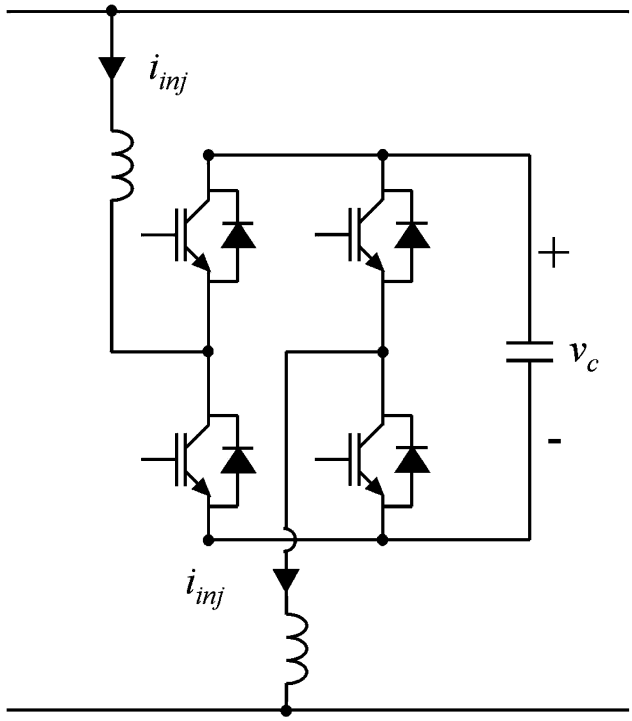

Fig. 7. H-bridge-based injection device circuit.

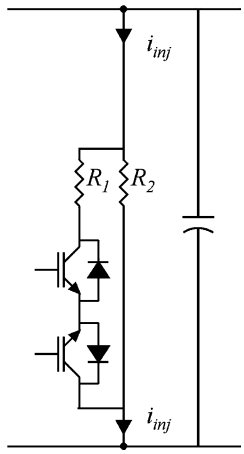

Fig. 8. Chopper injection circuit.

A. H-Bridge Circuit

Fig. 7 shows how the current injection can be accomplished with an H-bridge circuit. When applying this circuit for current

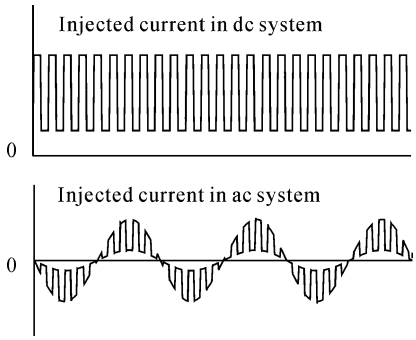

Fig. 9. Injected current waveforms in dc and ac systems.

injection, a current-regulated PWM method such as hysteresis modulation or delta modulation [19] can be used to ensure the appropriate currents. The advantage of the active H-bridge converter is accurate control of the injected currents. However, this control means that the switching frequency of the inverter must be several times the highest frequency component of the injected current. For this reason, the H-bridge circuit is recommended for low-voltage systems where higher frequency transistors can be used.

B. Chopper Circuit

The H-bridge circuit generates an injection current using techniques similar to a single-phase inverter, where the dc power source is the dc capacitor link. The injected current is controlled to the desired current. The chopper circuit, however, generates the injection current by creating a variable impedance path across two phases of the system. Since the line-to-line voltage contains the fundamental frequency ω_e, the variable impedance is designed with switching frequency $|\omega_s \pm 2\omega_e|$ to satisfy (17). As shown in Fig. 8, the chopper circuit consists of two resistive branches, and a bidirectional switch is connected in series with one of the branches. By gating the switch ON and OFF, the equivalent impedance of the circuit alternates between R_2 and $R_1 \| R_2$. The values of resistors R_1 and R_2 do not have to be the same. Mathematical analysis shows that when the value of R_2 is infinite, the fundamental injection has a smaller ratio, as detailed in the Appendix. In the following simulation and laboratory results, the R_2 branch is chosen to be an open circuit. The capacitor branch shown in Fig. 8 is small in value and operates as a snubber to extinguish voltage spikes caused by switching. This is necessary in typical power systems where the source and load are inductive in nature. Since the capacitive impedance is small, it does not significantly affect the impedance measurement.

Appropriate switching patterns, together with the fundamental line-to-line voltages across the circuit, create a current that flows from one line to the other. In this study, the bidirectional switch is controlled with square waves that have a fixed 50% duty cycle. The relationship between the square-wave impedance and desired injected current is given in the Appendix.

The primary advantage of the chopper circuit is that the switching frequency is set to $|\omega_s \pm 2\omega_e|$, which is very low compared to the H-bridge circuit method. Therefore, this circuit is more suitable for medium-voltage systems where the transistor switching frequency is limited. The primary disadvantage is that the injected current will have considerable harmonics. However, these are mathematically removed by the FFT process.

TABLE I
INDUCTION MACHINE PARAMETERS

$r_s = 0.4\ \Omega$	$P = 4$	$r_r' = 0.227\ \Omega$
$L_{ls} = 5.73$mH	$L_M = 64.4$ mH	$L_{lr}' = 4.64$ mH

The injection frequency of the proposed method is a function of the fundamental frequency. This means that for measuring frequencies well below the fundamental, the injected current is at a frequency close to the fundamental, which is easier to generate and leads to shorter data logging times. For example, measuring the impedance at 0.1 Hz with the proposed method uses a switching frequency around $2f_e \pm 0.1$ Hz, while typical three-phase injection methods requires near-zero switching frequencies, which may be problematic in hardware implementation.

The idealized injected currents of the chopper circuit for dc and ac systems have example waveforms shown in Fig. 9. In dc systems, the injected current is proportional to the resistor value, so it is also a square waveform. In ac systems, a square wave with a frequency of $|\omega_s \pm 2\omega_e|$ modulated by the fundamental frequency will result in the $|\omega_s \pm \omega_e|$ frequency terms.

V. COMPUTER SIMULATION RESULTS

A line-to-line chopper circuit injection was simulated for the system shown in Fig. 10, using the advanced continuous simulation language (ACSL) [20]. A fixed-frequency (60 Hz) ac power source with input inductors is used to represent a utility grid or a synchronous generator. The system consists of a back-to-back rectifier/inverter feeding an induction motor load. PWM filters are added between the ac source and rectifier, and between the inverter and motor load. The ac source has an inductance of $L_s = 0.46$ mH and a line-to-neutral terminal voltage of 120 V. Both PWM filters have parameters of $R_{f1} = R_{f2} = 10.86\ \Omega$, $L_{f1} = L_{f2} = 1.2$ mH, and $C_{f1} = C_{f2} = 5.95\ \mu$F. The dc-link capacitance is $C_{\rm dc} = 3500\ \mu$F. The induction motor is a 3.7-kW machine with d–q model [21] parameters listed in Table I. In this system, the rectifier is controlled [16] with a constant modulation index of $m = 0.88$ and constant phase angle relative to the source voltage of $\phi_v = -3.55^{\rm o}$. The inverter operates with a constant frequency of 60 Hz and a modulation index of 0.97. The induction motor speed is set to 1750 r/min for rated operation.

Injection of shunt current for impedance measurement is accomplished using the chopper circuit shown in Fig. 8, which is capable of measuring at ac or dc interfaces. For ac impedance measurement, the injection circuit was placed between the source and input filter. For dc impedance measurement, the chopper circuit measures impedance at the output of the rectifier (before the dc-link capacitor). The source impedance and load admittance at dc are shown in Fig. 11. The frequency was swept from 0.1 to 4995 Hz, and the source impedance and load admittance was extracted for each frequency. Two simulation sets are

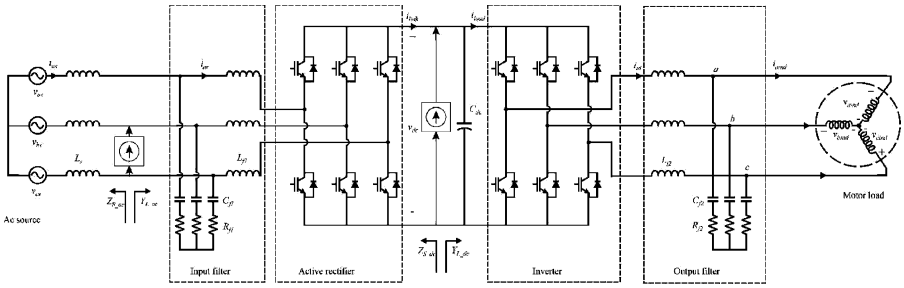

Fig. 10. Example system for impedance measurement demonstration.

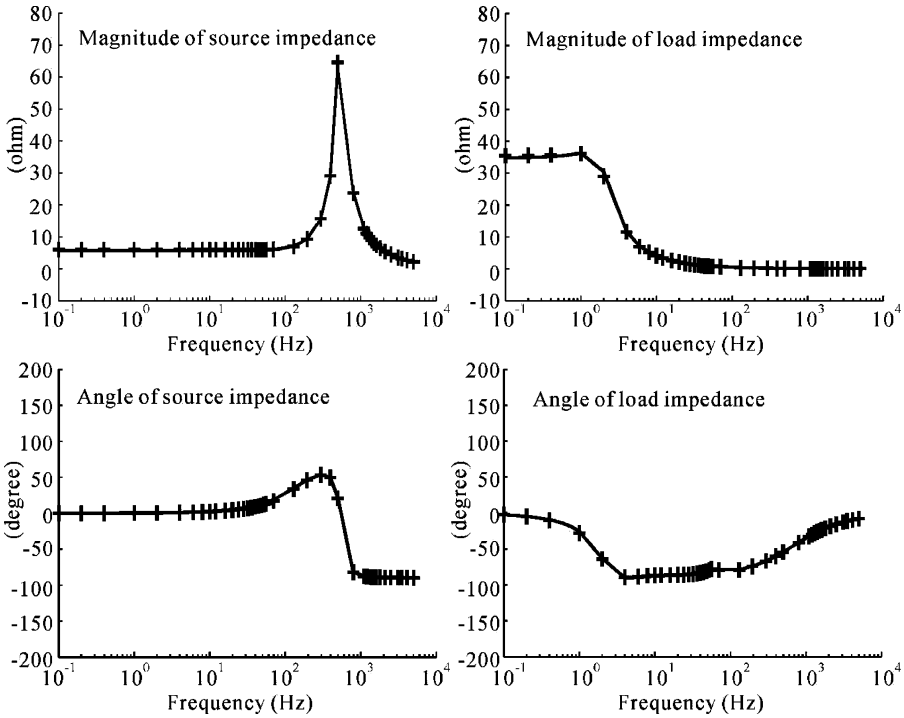

Fig. 11. DC impedances determined in simulation.

used for ac and dc impedances separately. Fig. 12 shows the ac source impedances and load admittance determined from simulation using the chopper circuit current injection. A Jacobian analysis was also applied in ACSL to obtain the small-signal $d-q$ impedance matrix [20] based on frequency-domain calculation about the operating point in state space by numerical perturbation. The $d-q$ impedance matrix was then used to compare with simulation results from the injected signal.

Fig. 11 shows the simulated magnitude and phase information of the impedances at the dc interface. Fig. 12 shows the four individual $d-q$ impedances determined at the ac interface of system in the form of real and imaginary parts. It is presented in this form because, at some frequencies, the magnitude is close to zero and the angle then loses meaning. Herein, the solid line of both plots denotes the Thevenin $d-q$ impedance and the "+" markers correspond to the points predicted from the injection methods. As can be seen, they appear identical, thus validating the impedance measurement method using a detailed simulation of the injection circuit and waveform processing outlined in Fig. 5.

VI. Laboratory Validation

A. Induction Motor Drive System

In order to validate the proposed method, a laboratory prototype of the system shown in Fig. 10 was assembled and tested together with a line-to-line chopper injection circuit. The chopper circuit was operating with $R_1 = 200\,\Omega$ and $R_2 = \infty$. The following sections describe the resulting measurements.

In the laboratory, the injection frequencies were swept from 0.3 to 4995 Hz at values corresponding to the simulation. To avoid the effects of system harmonics on the injection signal measurement, measurement at frequencies that are multiples of system fundamental frequency were avoided during the test. The data acquisition device sampling frequency and resolution are high enough that the small injection signal could be extracted without degradation of accuracy.

The first laboratory measurement involved the shunt-connected chopper circuit for measurement of the dc impedance. As with the simulation results, the magnitude and phase of the impedances are shown in the graphs. The ideal Jacobian

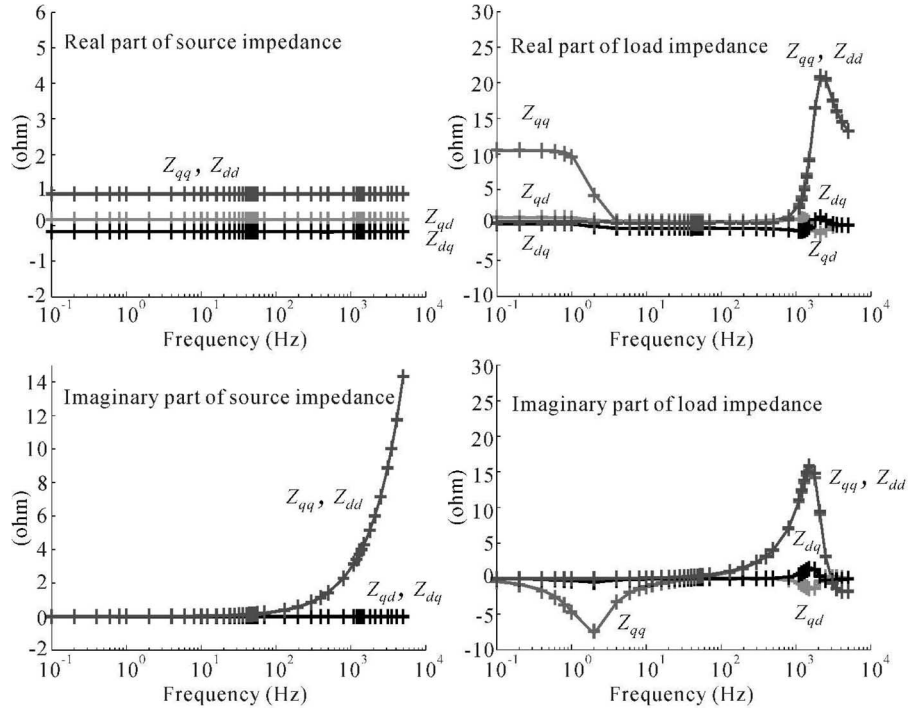

Fig. 12. AC impedances determined in simulation.

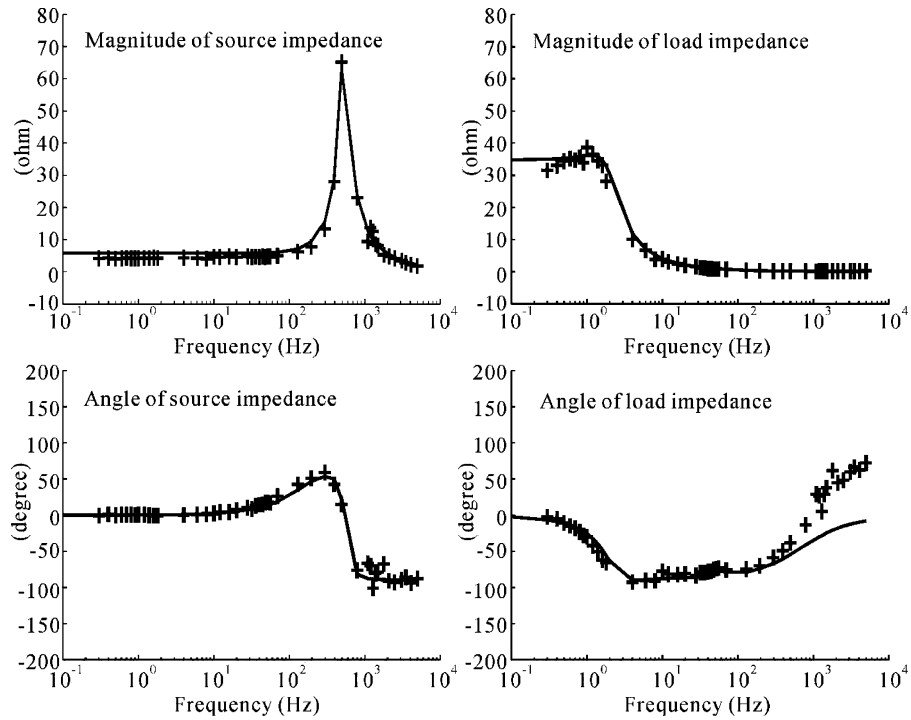

Fig. 13. Measured dc system impedances.

prediction of the system impedance was plotted as the solid line. The +'s are from the line-to-line injection measurements using the chopper circuit. As can be seen from Fig. 13, the dc impedance extracted from laboratory measurements is consistent with the ideal impedance or simulated results with the exception of the magnitude of load at low frequency and phase of load at high frequency. The latter discrepancy is because both the real part and the imaginary part of the load impedance are close to zero, and the phase values become very sensitive to a small measurement error. However, when the magnitude of the impedance is

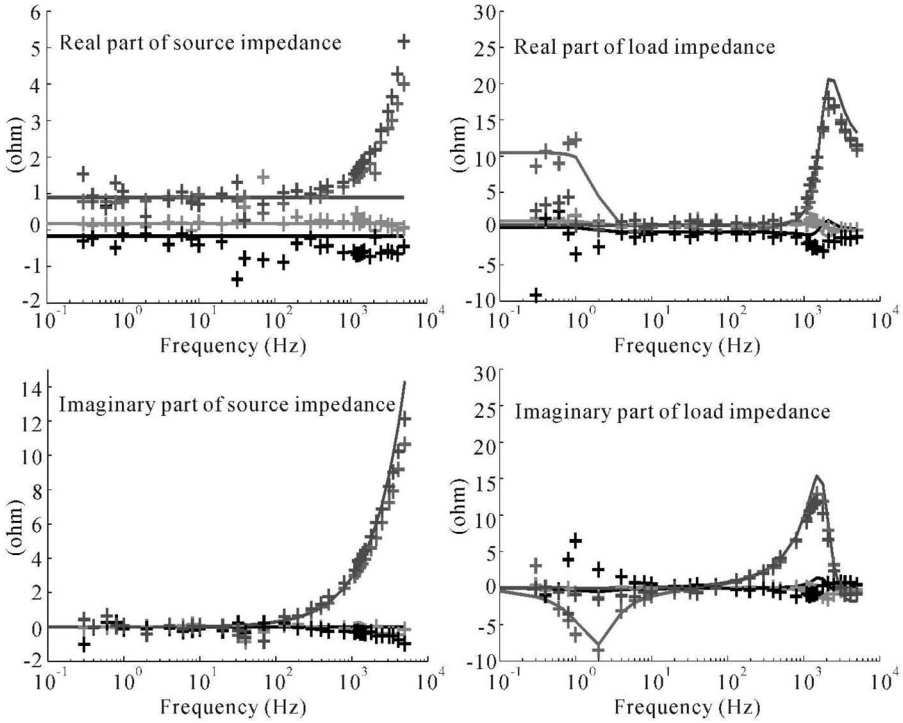

Fig. 14. Measured ac system impedances.

close to zero, the phase becomes insignificant. The mismatch at low frequencies is because there is a dc machine driving the inductor motor in the laboratory. The control loop for this dc machine includes a speed proportional integral (PI) controller, with a commanded output current, and an armature current PI controller. The model for this is approximately replaced with an induction motor running at constant speed in the simulation.

Fig. 14 shows the ac impedance measurement results. The traces and scales for this figure are the same as the simulated results shown in Fig. 12. Overall, the measured impedances are in good agreement with the ideal impedances. The discrepancy in the real part of the source impedance at high frequency is primarily due to the existence of nonideal resistance that varies with frequency. In the laboratory setup, an Elgar-SW5250A power supply [22] was programmed to provide the three-phase voltage. An output impedance curve from the manufacturer shows an increase of resistance value as frequency increases with a magnitude that accounts for the measured error. The real part of Z_{qd} and Z_{dq} has some small error, which is acceptable, because the values themselves are very small.

At low frequencies, discrepancies in the load impedance are seen at low frequencies. However, the measured value of Z_{qq} is shown to be close to the ideal value. Since the magnitude of Z_{qq} is much greater than the other impedances, it will be dominated in terms of ac system stability criteria [12]. Therefore, these measurements are still useful in predicting system stability.

B. Navy Ship System Inverter

As a final experimental test, the chopper circuit was used to measure impedance of a standard shipboard inverter. In this system, the inverter was supplying 450-V to a 100-kW three-phase resistive load. The chopper circuit was placed between the inverter and load, and impedance measurement was obtained for frequencies from 2 to 500 Hz. Good signal integrity was obtained, and the source and load impedances had a reasonable variation with frequency. Herein, the impedance information was combined to form the Nyquist plot. Fig. 15(a) shows a photograph of the chopper circuit and Fig. 15(b) shows the resulting Nyquist plot. There are two paths in the plot corresponding to the two eigenvalues. They start at the center and spiral outward as the measurement frequency is increased. Since the eigenvalues are far from the -1 point and no encirclement is seen, the system is seen to be very stable.

VII. Conclusion

As more power-electronics-based conversion is incorporated into naval shipboard power systems, stability has become a major concern. Research into ac system stability using the small-signal impedances of the $d-q$ model is a relatively new concept when compared to dc stability. Recent research has defined stability criterion for ac systems, and methods of ac impedance measurement have been presented. This paper introduced a new method of ac impedance measurement, whereby a chopper circuit creates a line-to-line disturbance between two phases. It was mathematically shown, as well as through simulation and laboratory measurements, that all of the necessary $d-q$ model information can be obtained using measurements from the line-to-line disturbances. The new impedance measurement circuit is simple to construct, suitable for both dc and ac impedance measurements, and applicable to medium-voltage systems.

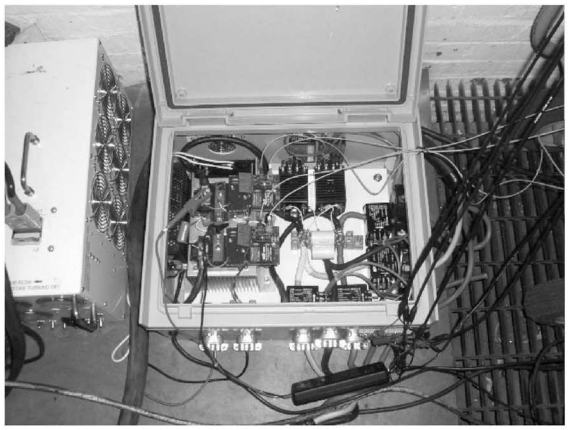

(a)

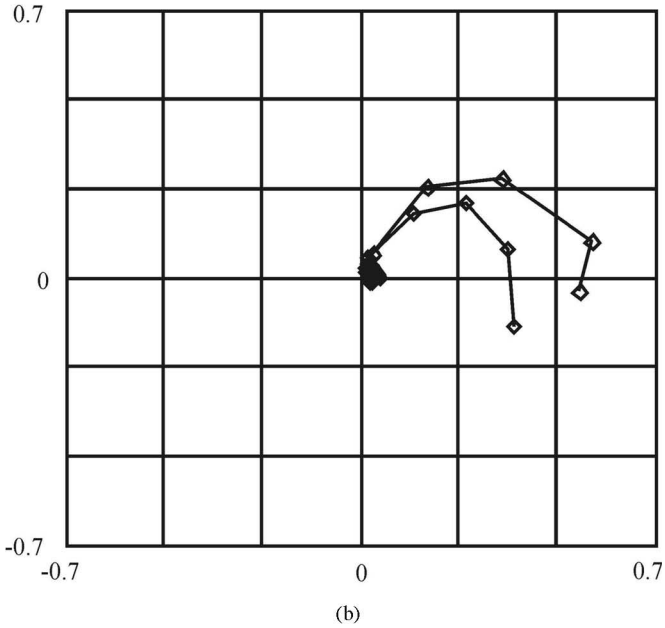

(b)

Fig. 15. Laboratory measurement at NSWC. (a) Photograph of impedance measurement device. (b) Nyquist plot of PCM-2 inverter output.

APPENDIX

The switching waveform for the chopper transistor command is a square wave that can be expressed by the sum of a series of the harmonics of the switching frequency

$$\mathrm{sw} = d + 2\sum_{k=1}^{\infty} \frac{\sin(k\pi d)}{k\pi}\cos(k\omega t) \tag{19}$$

where d is the duty cycle, k is the harmonic number, and ω is the switching frequency, which was based on the desired injection frequency and fundamental frequency as $|\omega_s \pm 2\omega_e|$.

The coefficient of each harmonic is $2\sin(k\pi d)/k\pi$ with an offset of d, the value of which will decrease as k increases. It can be seen that the term at the switching frequency is dominant. When the duty cycle d is set to 50%, this term will have maximum amplitude.

The equivalent resistance of the chopper circuit in Fig. 8 is

$$R = \mathrm{sw}\,(R_1 \| R_2) + (1-\mathrm{sw})R_2 = R_2 - \mathrm{sw}\frac{R_2^2}{R_1+R_2}. \tag{20}$$

The equivalent admittance is obtained by taking the inverse of equivalent resistance. Considering two typical cases, the admittances can be calculated as

$$\begin{aligned} Y_{\mathrm{case1}} &= \frac{1}{R} = \frac{2}{R_1(2-\mathrm{sw})} = \frac{1+\mathrm{sw}}{R_1} \\ Y_{\mathrm{case2}} &= \frac{\mathrm{sw}}{R_1} \end{aligned} \tag{21}$$

where case 1 involves $R_1 = R_2$ and case 2 involves $R_2 = \infty$. Considering the dominant terms of the waveform, the injected current in ac systems and dc systems becomes

$$\begin{aligned} i_{\mathrm{inj\_ac}} &= v_{bc}Y \\ &= \frac{V_{ll}\cos(\omega_e t)}{R_1}\left(a + d + 2\frac{\sin(\pi d)}{\pi}\cos(\omega_s t \pm 2\omega_e t)\right) \\ &= \frac{V_{ll}}{R_1}(a+d)\cos(\omega_e t) \\ &\quad + \frac{V_{ll}\sin(\pi d)}{\pi R_1}\cos(\omega_s t \pm 3\omega_e t) + \cdots \\ &\quad + \frac{V_{ll}\sin(\pi d)}{\pi R_1}\cos(\omega_s t \pm \omega_e t) \end{aligned} \tag{22}$$

$$\begin{aligned} i_{\mathrm{inj\_dc}} &= v_{\mathrm{dc}}Y = V_{\mathrm{dc}}\frac{a + d + 2\,(\sin(\pi d)/\pi)\cos(\omega_s t)}{R_1} \\ &= \frac{V_{\mathrm{dc}}}{R_1}(a+d) + \frac{V_{dc}2\sin(\pi d)}{\pi R_1}\cos(\omega_s t) \end{aligned} \tag{23}$$

where a is equal to 1 for case 1 and 0 for case 2.

The last term of (22) is exactly the desired injection current defined in (17). Although the expression of (22) has more terms than needed, these terms will be mathematically removed by the FFT technique during data processing. Equations (22) and (23) show that the fundamental injection in case 2 has a smaller ratio when a is zero.

ACKNOWLEDGMENT

The authors wish to express their appreciation to R. Dietrich and J. Yuen at the Naval Surface Warfare Center, Philadelphia, PA, for supporting this project.

REFERENCES

[1] R. D. Middlebrook, "Input filter considerations in design and application of switching regulators," in *Proc. IEEE Ind. Appl. Soc. Conf.*, Oct. 1976, pp. 91–107.

[2] Y. Panov and M. Jovanovic, "Practical issues of input/output impedance measurements in switching power supplies and application of measured data to stability analysis," in *Proc. IEEE Appl. Power Electron. Conf.*, Mar. 2005, vol. 2, pp. 1339–1345.

[3] R. E. Serrano-Finetti and R. Pallas-Areny, "Output impedance measurement in power sources and conditioners," in *Proc. IEEE Instrum. Meas. Technol. Conf.*, May 2007, pp. 1–5.

[4] S. D. Sudhoff, K. A. Corzine, S. F. Glover, H. J. Hegner, and H. N. Robey, Jr., "DC link stabilized field oriented control of electric propulsion systems," *IEEE Trans. Energy Convers.*, vol. 13, no. 1, pp. 27–33, Mar. 1998.

[5] S. D. Sudhoff, S. F. Glover, P. T. Lamm, D. H. Schmucker, and D. E. Delisle, "Admittance space stability analysis of power electronic systems," *IEEE Trans. Aerosp. Electron. Syst.*, vol. 36, no. 3, pp. 965–973, Jul. 2000.
[6] A. Emadi, A. Khaligh, C. H. Rivetta, and G. A. Williamson, "Constant power loads and negative impedance instability in automotive systems: Definition, modeling, stability and control of power," *IEEE Trans. Veh. Technol.*, vol. 55, no. 4, pp. 1112–1125, Jul. 2006.
[7] X. Feng, J. Liu, and F. C. Lee, "Impedance specifications for stable dc distributed power systems," *IEEE Trans. Power Electron.*, vol. 17, no. 2, pp. 157–162, Mar. 2002.
[8] C. M. Wildrick, F. C. Lee, B. H. Cho, and B. Choi, "A method of defining the load impedance specification for a stable distributed power system," *IEEE Trans. Power Electron.*, vol. 10, no. 3, pp. 280–285, Mar. 1995.
[9] J. Liu, X. Feng, F. C. Lee, and D. Borojevich, "Stability margin monitoring for dc distributed power systems via current/voltage perturbation," in *Proc. IEEE Appl. Power Electron. Conf.*, 2001, pp. 745–751.
[10] P. Xiao, G. K. Venayagamoorthy, and K. A. Corzine, "A novel impedance measurement technique for power electronic systems," in *Proc. IEEE Power Electron. Spec. Conf.*, Jun. 2007, pp. 955–960.
[11] J. Sun, "Input impedance analysis of single-phase PFC converters," *IEEE Trans. Power Electron.*, vol. 20, no. 2, pp. 308–314, Mar. 2005.
[12] M. Belkhayat, "Stability criteria for ac power systems with regulated loads," Ph.D. dissertation, Purdue Univ., West Lafayette, IN, Dec. 1997.
[13] M. Belkhayat and M. L. Williams, "Impedance extraction techniques for dc and ac systems," presented at the Naval Symp. Electric Mach., Philadelphia, PA, Dec. 2000.
[14] P. J. Kwasniok, M. D. Bui, A. J. Kozlowski, and S. S. Stanislaw, "Technique for measurement of powerline impedances in the frequency range from 500 kHz to 500 MHz," *IEEE Trans. Electromagn. Compat.*, vol. 35, no. 1, pp. 87–90, Feb. 1993.
[15] B. Palethorpe, M. Sumner, and D. W. P. Thomas, "Power system impedance measurement using a power electronic converter," in *Proc. IEEE Conf. Harmonics Quality Power*, Oct. 2000, vol. 1, pp. 208–213.
[16] Y. L. Familiant, K. A. Corzine, J. Huang, and M. Belkhayat, "AC impedance measurement techniques," in *Proc. IEEE Electric Mach. Drive Conf.*, May 2005, pp. 1850–1857.
[17] J. Huang and K. A. Corzine, "AC impedance measurement by line-to-line injected current," in *Proc. IEEE Ind. Appl. Soc. Conf.*, Oct. 2006, vol. 1, pp. 300–306.
[18] S. D. Sudhoff, B. Loop, J. Byoun, and A. Cramer, "A new procedure for calculating immittance characteristics using detailed computer simulation," in *Proc. IEEE Power Electron. Spec. Conf.*, Jun. 2007, pp. 901–908.
[19] K. A. Corzine and J. R. Baker, "Multi-level voltage-source duty-cycle modulation: Analysis and implementation," *IEEE Trans. Ind. Electron.*, vol. 49, no. 5, pp. 1009–1016, Oct. 2002.
[20] *Advanced Continuous Simulation Language (ACSL Reference Manual),* Mitchell & Gauthier Assoc., 11th edition, 1995.
[21] P. C. Krause, O. Wasynczuk, and S. D. Sudhoff, *Analysis of Electric Machinery and Drive Systems*. Piscataway, NJ: IEEE Press, 2002.
[22] *SmartWave Switching Amplifier Operation Manual*, Elgar Corp., San Diego, CA, 2002.

Jing Huang (S'04) received the B.S.E.E. degree from Nanchang University, Nanchang, China, in 1997, the M.S.E.E. degree from North China Electrical Power University, Beijing, China, in 2000, and the second M.S.E.E. degree from the University of Missouri, Rolla, in 2005. She is currently working toward the Ph.D. degree at Missouri University of Science and Technology, Rolla.

From 2000 to 2003, she was with Beijing Sifang Automation Corporation Ltd. Her current research interests include power electronics, multilevel converters, electrical machinery, and motor controls.

Keith A. Corzine (S'92–M'97) received the B.S.E.E., M.S.E.E., and Ph.D. degrees from the University of Missouri, Rolla, in 1992, 1994, and 1997, respectively.

From 1997 to 2004, he was at the University of Wisconsin, Milwaukee. He is currently a Professor at Missouri University of Science and Technology, Rolla. His current research interests include power electronics, motor drives, naval ship propulsion system, and electric machinery analysis.

Mohamed Belkhayat received the Ph.D. degree in electrical engineering from Purdue University, West Lafayette, IN.

He was at the Naval Postgraduate School and the Naval Academy. He is currently a Research Engineer with Northrop Grumman Newport News, Washington, DC. His current research interests include modeling, simulation, and analysis of advanced naval power systems.